

Left Ventricular Failure Produces Profound Lung Remodeling and Pulmonary Hypertension in Mice : Heart Failure Causes Severe Lung Disease

Yingjie Chen, Haipeng Guo, Dachun Xu, Xin Xu, Huan Wang, Xinli Hu, Zhongbing Lu, Dongmin Kwak, Yawei Xu, Roland Gunther, Yuqing Huo and E. Kenneth Weir

Hypertension. 2012;59:1170-1178; originally published online April 16, 2012;
doi: 10.1161/HYPERTENSIONAHA.111.186072

Hypertension is published by the American Heart Association, 7272 Greenville Avenue, Dallas, TX 75231
Copyright © 2012 American Heart Association, Inc. All rights reserved.
Print ISSN: 0194-911X. Online ISSN: 1524-4563

The online version of this article, along with updated information and services, is located on the World Wide Web at:

<http://hyper.ahajournals.org/content/59/6/1170>

Data Supplement (unedited) at:

<http://hyper.ahajournals.org/content/suppl/2012/04/16/HYPERTENSIONAHA.111.186072.DC1.html>

Permissions: Requests for permissions to reproduce figures, tables, or portions of articles originally published in *Hypertension* can be obtained via RightsLink, a service of the Copyright Clearance Center, not the Editorial Office. Once the online version of the published article for which permission is being requested is located, click Request Permissions in the middle column of the Web page under Services. Further information about this process is available in the [Permissions and Rights Question and Answer](#) document.

Reprints: Information about reprints can be found online at:
<http://www.lww.com/reprints>

Subscriptions: Information about subscribing to *Hypertension* is online at:
<http://hyper.ahajournals.org/subscriptions/>

Left Ventricular Failure Produces Profound Lung Remodeling and Pulmonary Hypertension in Mice

Heart Failure Causes Severe Lung Disease

Yingjie Chen, Haipeng Guo, Dachun Xu, Xin Xu, Huan Wang, Xinli Hu, Zhongbing Lu, Dongmin Kwak, Yawei Xu, Roland Gunther, Yuqing Huo, E. Kenneth Weir

Abstract—Chronic left ventricular failure causes pulmonary congestion with increased lung weight and type 2 pulmonary hypertension. Understanding the molecular mechanisms for type 2 pulmonary hypertension and the development of novel treatments for this condition requires a robust experimental animal model and a good understanding of the nature of the resultant pulmonary remodeling. Here we demonstrate that chronic transverse aortic constriction causes massive pulmonary fibrosis and remodeling, as well as type 2 pulmonary hypertension, in mice. Thus, aortic constriction-induced left ventricular dysfunction and increased left ventricular end-diastolic pressure are associated with a ≤ 5.3 -fold increase in lung wet weight and dry weight, pulmonary hypertension, and right ventricular hypertrophy. Interestingly, the aortic constriction-induced increase in lung weight was not associated with pulmonary edema but resulted from profound pulmonary remodeling with a dramatic increase in the percentage of fully muscularized lung vessels, marked vascular and lung fibrosis, myofibroblast proliferation, and leukocyte infiltration. The aortic constriction-induced left ventricular dysfunction was also associated with right ventricular hypertrophy, increased right ventricular end-diastolic pressure, and right atrial hypertrophy. The massive lung fibrosis, leukocyte infiltration, and pulmonary hypertension in mice after transverse aortic constriction clearly indicate that congestive heart failure also causes severe lung disease. The lung fibrosis and leukocyte infiltration may be important mechanisms in the poor clinical outcome in patients with end-stage heart failure. Thus, the effective treatment of left ventricular failure may require additional efforts to reduce lung fibrosis and the inflammatory response. (*Hypertension*. 2012;59:1170-1178.) • [Online Data Supplement](#)

Key Words: pulmonary hypertension ■ transverse aortic constriction ■ pulmonary vascular morphology

Pulmonary hypertension (PH) secondary to left ventricular systolic or diastolic dysfunction or to valvular disease is classified as type 2 PH.¹ The occurrence of PH in the setting of elevated left atrial pressure (pulmonary venous hypertension) has been recognized since the 1940s. In 1945, Cournand et al² published the pulmonary artery pressure trace in a case of “rheumatic valvulitis with hypertension in the lesser circulation.” The pulmonary artery systolic pressure was >80 mmHg. It is predicted that $\leq 60\%$ of patients with severe left ventricular (LV) systolic dysfunction and $\leq 70\%$ of patients with LV diastolic dysfunction may develop PH, but the detailed pulmonary remodeling in type 2 PH is not well defined. The presence of PH in these patients is associated with a worse prognosis.^{3–6} In view of the growing prevalence of LV systolic and diastolic failure, the clinical importance of

type 2 PH is becoming more prominent. Here we report a dramatic increase of lung weight, massive pulmonary fibrosis, leukocyte infiltration, profound vascular remodeling, type 2 PH, and right ventricular dysfunction in mice in response to LV systolic pressure overload produced by chronic transverse aortic constriction (TAC). However, the marked increase of lung weight 4 weeks post-TAC in mice with severe LV dysfunction was not the result of an increase of lung water content. Our findings suggest that the effective treatment of LV end-stage heart failure may also require additional efforts to reduce lung fibrosis and the inflammatory response.

Materials and Methods

Please see the online-only Data Supplement for the detailed Methods section.

Received October 12, 2011; first decision November 13, 2011; revision accepted March 22, 2012.

From the Lillehei Heart Institute and the Cardiovascular Division (Y.C., H.G., D.X., X.X., H.W., X.H., Z.L., D.K., Y.H.), University of Minnesota Medical School, Minneapolis, MN; Key Laboratory of Cardiovascular Remodeling and Function Research (H.G.), Chinese Ministry of Education and Chinese Ministry of Health, Qilu Hospital, Shandong University, Shandong, China; Department of Cardiology (D.X., Y.X.), Shanghai Tenth People's Hospital of Tongji University, Shanghai, China; Research Animal Resources (R.G.), University of Minnesota, Minneapolis, MN; Department of Medicine (E.K.W.), University of Minnesota and Veterans Affairs Medical Center, Minneapolis, MN.

H.G. and D.X. contributed equally to this work.

The online-only Data Supplement is available with this article at <http://hyper.ahajournals.org/lookup/suppl/doi:10.1161/HYPERTENSIONAHA.111.186072/-DC1>.

Correspondence to Yingjie Chen, Lillehei Heart Institute and Cardiovascular Division, University of Minnesota, 420 Delaware St SE, Minneapolis, MN 55455. E-mail chenx106@umn.edu

© 2012 American Heart Association, Inc.

Hypertension is available at <http://hyper.ahajournals.org>

DOI: 10.1161/HYPERTENSIONAHA.111.186072

Experimental Animals

C57B6J (Jackson Laboratory) mice were used for the described studies. This study was approved by the University of Minnesota Institutional Animal Care and Use Committee. Study was conducted in accordance with the National Institutes of Health Guide for the Care and Use of Laboratory Animals.

Induction of PH with TAC or Hypoxia in Mice

Male mice at age 10 to 14 weeks were used for the minimally invasive TAC procedure, as we have described previously.^{7–10} For induction of PH with hypoxia, mice were exposed to hypobaric hypoxia.⁹

Sample Preparation

Heart, lung, and other major organs were harvested and weighed. The ratio of right ventricle (RV) weight to left ventricle (LV) + septum (S) was calculated as an index of RV hypertrophy.^{9,11} The airways of the upper right lobe were perfused and fixed in 10% buffered formalin for histological analysis. Visual comparable inflation of the lung lobes was observed in all of the tissues.

Measure Lung Water Content and RT-PCR

Lung (lower right lobe) wet weight was first determined. The lung tissue was then dried at 58°C to a constant weight. The dry weight of lung tissue was then determined. The relative water content of lung tissue was calculated using the following equation: lung water content = (lung wet weight – lung dry weight)/lung wet weight × 100%. The sequences of the primers used for quantitative real-time PCR are provided in Table S1 (available in the online-only Data Supplement).

Results

TAC-Induced Increases of Lung Weight and RV Hypertrophy Are Related to the Degree of LV Failure

Previous studies demonstrated that TAC-induced LV hypertrophy and LV dysfunction are associated with increases in lung weight,^{8,9,12,13} left atrial weight,⁸ and RV weight. However, no study has carefully investigated the relationships of these parameters. To further understand the cardiac and pulmonary changes occurring secondary to LV dysfunction, we determined the relationships of LV hypertrophy, LV dysfunction, and increases of left atrial weight, lung weight, and RV weight in a group of mice after moderate TAC-induced LV hypertrophy and dysfunction. As demonstrated in Figure 1, the increases of LA weight, lung weight, RV weight, and their ratio to body weight after TAC are significantly related to the increase of LV weight or its ratio to body weight in these mice, but their relationships are in a nonlinear fashion (Figure 1A through 1C). However, the decrease of LV ejection fraction was correlated to the increase of the ratio of LV weight:body weight in a largely linear fashion (Figure 1D). The increases of LA weight, lung weight, RV weight, and their ratio to body weight after TAC are all significantly correlated with the decrease of LV ejection fraction (Figure 1E through 1G). Increase of the ratio of RV weight:body weight (a reliable marker for PH) was also correlated to the increase of the ratio of lung weight:body weight in a nonlinear fashion (Figure 1H).

TAC-Induced Severe LV Dysfunction Is an Effective Cause of Increases in Lung Weight, PA, and RV Hypertrophy in Mice

To further determine whether the degree of LV failure affects the severity of TAC-induced lung remodeling and RV hyper-

trophy, mice after TAC were divided into a severe LV failure group (HF; when LV ejection fraction is <50%) or mild/moderate heart failure group (M-HF; when LV ejection fraction is >50%). The data obtained from these groups were further compared with the data obtained from a group of control C57B6J mice (control) and a group of C57B6J mice subjected to 3 weeks of hypoxia (Figure 2 and Table S1). As shown in Figure 2, hypoxia causes no LV dysfunction and no LV or LA hypertrophy but did cause a small but significant increase in the ratio of lung weight:body weight and ≈50% RV hypertrophy. HF and M-HF mice had decreased LV ejection fraction, $42.7 \pm 1.85\%$ and $66.2 \pm 3.42\%$, respectively (control LV ejection fraction was $80.1 \pm 1.07\%$; Figure 2A). Both HF and M-HF mice had significant LV hypertrophy, LA hypertrophy, and a significant increase in the ratio of lung weight:body weight (Figure 2B through 2D), although these increases were significantly greater in the HF group. Interestingly, all of the HF mice had an increase of lung weight >50%, whereas only 1 of 12 M-HF mice had lung weight increased >50%, indicating that lung weight is a highly reliable marker for LV dysfunction. The M-HF group had no RV hypertrophy and a minimal increase of lung weight, whereas the HF group had a dramatic increase of lung weight and significant RV hypertrophy (Figure 2D and 2E). Neither the hypoxia nor the M-HF group develop right atrial hypertrophy, whereas the HF group had significant right atrial hypertrophy (HF 0.22 ± 0.02 versus M-HF 0.15 ± 0.01 versus hypoxia 0.13 ± 0.01 ; Figure 2F), indicating that RV dysfunction developed in the HF group but not in the hypoxia or M-HF groups.

LV and RV hemodynamics in the control group, the TAC-induced M-HF or HF groups, and the hypoxia group are presented in Figure 2G through 2L and Table S3. Both the M-HF and HF groups had significant increases in LV systolic pressure. As compared with the M-HF group, the HF group had a significantly smaller increase in LV systolic pressure (Figure 2G), reaffirming reduced LV function in this group. Both the M-HF and HF groups had significant increases in LV end-diastolic pressure, decreased LV contractility, and increased RV systolic pressure. However, these changes were more significant in the HF group (Figure 2H through 2L). The TAC-induced HF group also had a significant increase in RV end-diastolic pressure. The right atrial hypertrophy in this group is consistent with the increased RV end-diastolic pressure and the occurrence of ascites in some of the mice. As expected, the hypoxia group had no significant alterations in LV pressure, LV end-diastolic pressure, or LV contractility (Figure 2G through 2I) but had a significant increase in RV systolic pressure and a small but significant increase in RV end-diastolic pressure (Figure 2K and 2L). The increase in RV pressure in the M-HF or HF groups was similar or greater to that in hypoxia-induced PH (Figure 2K to 2L), indicating that TAC-induced HF is an effective cause of PH in mice.

We further determined the degree of RV fibrosis and cardiac myocyte hypertrophy in response to hypoxia, TAC-induced M-HF, or TAC-induced HF. Consistent with the severity of RV hypertrophy in the hypoxia and HF groups, histological analysis indicated a significant increase in RV

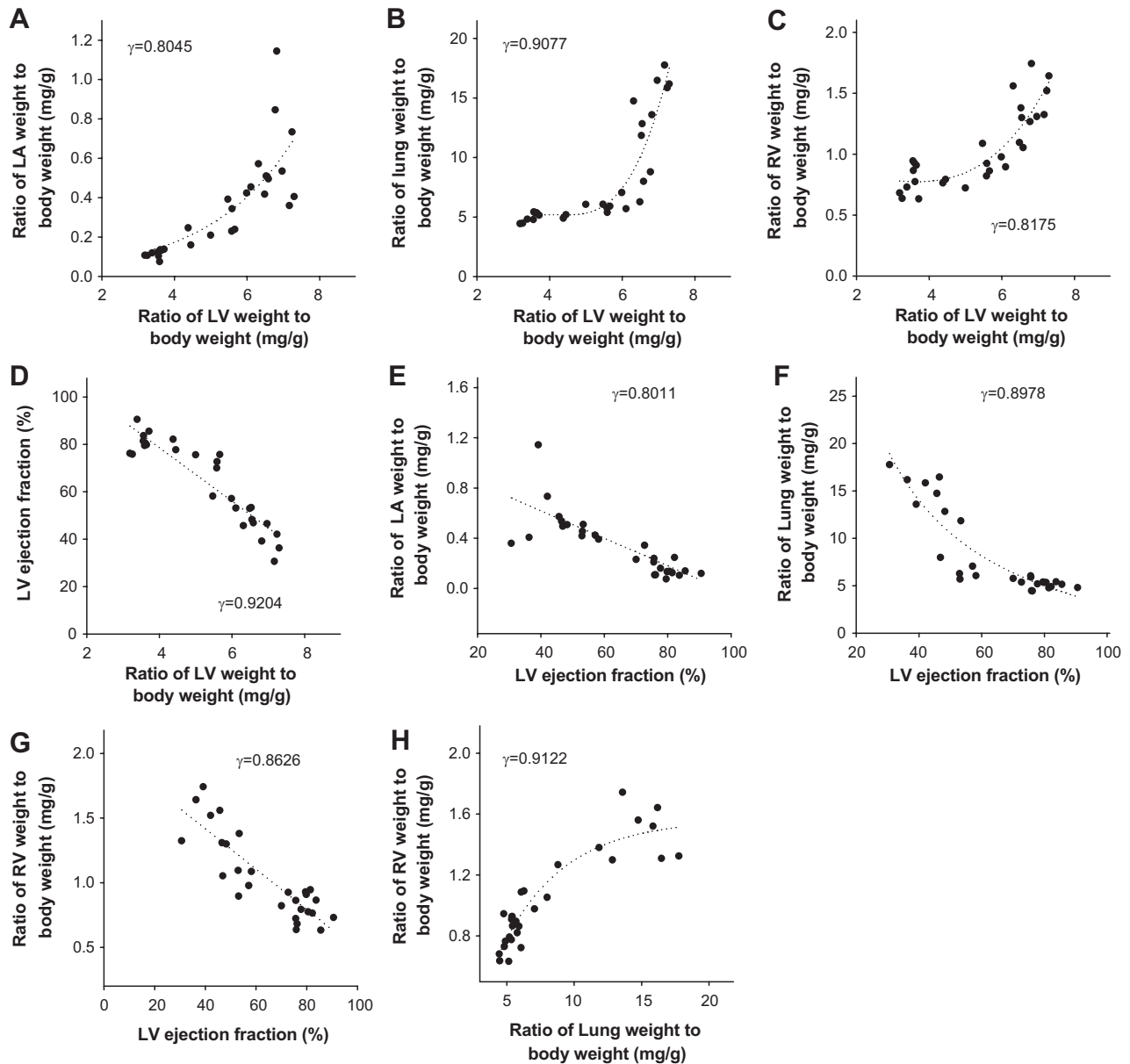


Figure 1. The transverse aortic constriction (TAC)-induced increases of lung weight and right ventricular (RV) hypertrophy are related to the degree of left ventricular (LV) hypertrophy and failure. **A** through **D**, Correlations between LV weight and LA weight, lung weight, RV weight, or LV ejection fraction. **E** through **G**, Correlations between LV ejection fraction and LA weight, lung weight, or RV weight. **H**, Correlation between increase of lung weight and RV weight.

fibrosis (Figure S1A and S1B) and cardiac myocyte cross-sectional area (Figure S1A and S1C) in these groups, indicating that both fibrosis and cardiac myocyte hypertrophy contributed to the RV hypertrophy.

TAC-Induced Increase in Lung Weight Is Not Merely the Result of Pulmonary Edema

LV failure often causes significant increases of lung weight, and this is a reliable marker for LV dysfunction.^{8,9,12,13} The increases in lung weight are commonly ascribed to pulmonary edema or increased interstitial fluid. To determine whether the increase in lung weight was a result of pulmonary edema, we determined the relative water content of lung tissue in the sham group, M-HF group, and HF group. Surprisingly, whereas the TAC-induced HF group had a

≈3-fold increase in lung weight, this was not the result of increased water content in the lung tissue (Figure 3A). This observation was highly reproducible in the TAC-induced HF model but contradicts the accepted concept of chronic congestion in heart failure.

TAC-Induced HF Causes Profound Lung Vascular Remodeling and Lung Fibrosis

We further determined the percentage of nonmuscularized, partially muscularized, and fully muscularized small arteries in mice under control conditions, after TAC-induced M-HF or HF, and after 3 weeks of hypoxia. TAC-induced M-HF or HF and hypoxia all caused increases in fully muscularized small arteries, but these increases were greater in the TAC-induced HF group than in the hypoxia or M-HF groups

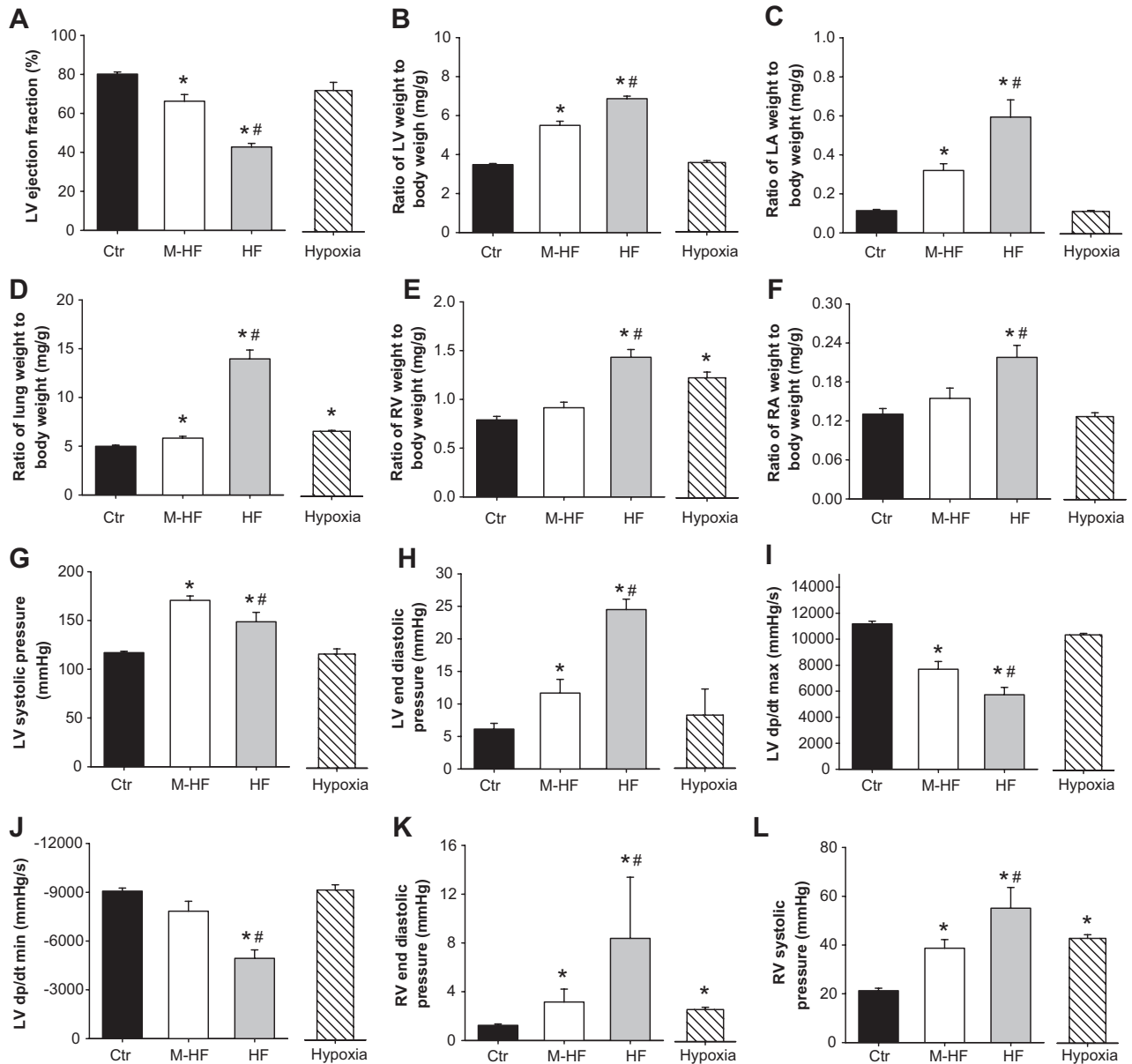


Figure 2. Alterations of heart and lung anatomic data and cardiac function in 4 experimental groups. **A**, Left ventricular (LV) ejection fraction in each group. **B**, Relative LV hypertrophy. **C**, LA hypertrophy. **D**, Increase of lung weight. **E**, Right ventricular (RV) hypertrophy. **F**, Right atrial (RA) hypertrophy. **G**, Heart failure (HF) group shows reduced LV systolic pressure as compared with mild/moderate heart failure (M-HF) group. **H**, HF group shows increased LV end-diastolic pressure as compared with other groups. **I** and **J**, HF group shows reduced LV contractility. **K**, M-HF and HF groups show increased end-diastolic RV pressure and **L** increased RV systolic pressure. * $P < 0.05$ vs control group; # $P < 0.05$ vs corresponding M-HF group.

(Figure 3B). The M-HF, HF, and hypoxia groups all had significant decreases in nonmuscularized small arteries, but these decreases were significantly greater in the HF group than in the other 2 groups (Figure 3B), indicating that TAC-induced HF is a highly effective model in causing PH and pulmonary vascular remodeling.

Interestingly, the HF group showed prominent pulmonary vascular and perivascular remodeling, as indicated by marked vascular wall thickening and vascular lesions (Figures 4 and S2 through S5). The HF group also showed thickened alveolar septa (Figure S2 through S4) and focal collapsed alveolar airspaces filled with fibroblasts (Figure S4 and S5), collagen (Figures 4 and S6 through S8), and leukocytes

(Figure 5A through 5C). Staining for smooth muscle α -actin was increased in the area with fibrosis (Figure S4), as in the lung vessels (Figure S4 and S5), in the HF group, indicating proliferation of smooth muscle cells and myofibroblasts. As compared with control and M-HF groups, the HF group also showed prominent vascular and perivascular fibrosis (Figure 4A through 4H) and broadly diffused lung collagen deposition in all of the HF mice (Figures S6 and 4D), together with patches of lung fibrosis in some of HF mice (Figure 4C, 4E, and 4I through 4K). In addition, data obtained from the whole lung (Figure 5A through 5C). Staining for smooth muscle α -actin was increased in the area with fibrosis (Figure S4), as in the lung vessels (Figure S4 and S5), in the HF group, indicating proliferation of smooth muscle cells and myofibroblasts. As compared with control and M-HF groups, the HF group also showed prominent vascular and perivascular fibrosis (Figure 4A through 4H) and broadly diffused lung collagen deposition in all of the HF mice (Figures S6 and 4D), together with patches of lung fibrosis in some of HF mice (Figure 4C, 4E, and 4I through 4K). In addition, data obtained from the whole lung

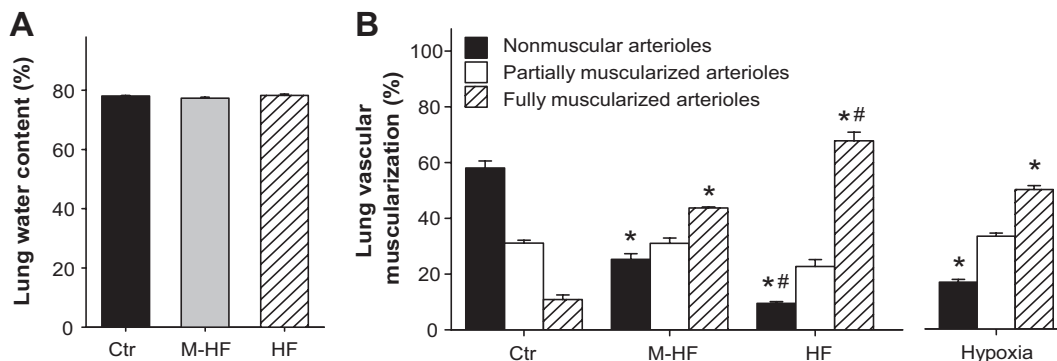


Figure 3. Chronic transverse aortic constriction (TAC) and hypoxia cause no pulmonary edema but cause pulmonary vascular remodeling. **A**, Chronic TAC-induced increase of lung weight is not related to pulmonary edema or water retention. **B**, Distribution of nonmuscular (■), partially muscularized (□), and fully muscularized (▨) small arteries in mice after chronic hypoxia or TAC-induced mild/moderate heart failure (M-HF) and TAC-induced heart failure (HF). * $P < 0.05$ vs control group; # $P < 0.05$ vs corresponding M-HF group.

Lung fibrosis, vascular fibrosis, and myofibroblast proliferation are often associated with increased transforming growth factor (TGF)- β signaling. In support of an increase in lung TGF- β signaling in HF mice, TGF- β mRNA was significantly increased in the TAC-induced HF group. However, the increase in TGF- β mRNA was similar between the hypoxia group and the TAC-induced HF group (Figure S9A). Western blot showed that TGF- β protein content was also increased in the M-HF and HF groups (Figure 6A and 6B). Consistent with the observed interstitial lung fibrosis, real-time quantitative PCR showed that both hypoxia and TAC-induced HF caused increases in lung collagen I and collagen III (Figure S9B and S9C), but these increases were markedly greater in the TAC-induced HF group than in the hypoxia group (Figure S9). Western blot showed that collagen I and collagen III protein contents were also increased in the M-HF and HF groups (Figure 6A, 6C, and 6D).

HF Causes Lung Inflammation

Histological analysis demonstrated accumulation of leukocytes and macrophages in the alveoli, inside the vessels, in the vascular wall of large vessels, and in the interstitial space of lung tissues obtained from the TAC-induced HF group (Figure 5A through 5C). The increased infiltration of macrophages was confirmed by staining with macrophage-specific marker Mac-2 (Figure 5B), whereas the infiltration of neutrophils was confirmed using a specific antibody against mouse neutrophil clone 7/4 (Figure 5C).¹⁴

In addition, the mRNA of the proinflammatory cytokines tumor necrosis factor 1 α , monocyte chemoattractant protein 1, and toll-like receptor 4 were all increased in lung tissues from the hypoxia, M-HF, and HF groups, and these increases were markedly greater in the TAC-induced HF group than in the other groups (Figure S9D through S9F). Interleukin 1 β , vascular cell adhesion molecule (VCAM), and intercellular adhesion molecule (ICAM) 1 were all increased in lung tissues from the hypoxia, M-HF, and HF groups, but the increases were similar (Figure S9G through S9I). Western blots showed that tumor necrosis factor 1 α , ICAM, and VCAM protein contents were also increased in M-HF and HF groups (Figure 6A and 6E through 6G).

Discussion

Here we report massive pulmonary fibrosis, vascular remodeling, type 2 PH, and right ventricular dysfunction in response to LV systolic pressure overload produced by chronic TAC in mice. Strikingly, the dramatic increase of lung weight in mice 4 weeks after TAC, with severe LV dysfunction, was not the result of an increase of lung water but was associated with massive lung fibrosis, leukocyte infiltration, and profound vascular remodeling. This observation was highly reproducible in the TAC-induced HF model but is contrary to the accepted concept of pulmonary edema or congestion in chronic heart failure. The prominence of lung fibrosis in this model may provide novel insights regarding the progression of, and clinical treatment for, end-stage LV dysfunction. The lung fibrosis and remodeling may be important mechanisms for the poor clinical outcome in patients of end-stage heart failure. Thus, the effective treatment of LV end-stage heart failure may also require additional efforts to reduce lung fibrosis and inflammatory response.

The increase in LV afterload caused by TAC leads to pathological LV hypertrophy, a decrease in LV ejection fraction, and an increase in LV end-diastolic pressure. The increased LV filling pressure resulted in impressive LA hypertrophy, an increase in pulmonary artery pressure, RV hypertrophy, and RV dysfunction, as indicated by increased RV end-diastolic pressure and right atrial hypertrophy. TAC-induced LV dysfunction also caused a dramatic increase in the percentage of fully muscularized small pulmonary arteries, marked lung fibrosis, myofibroblast proliferation, and leukocyte infiltration. The potential mechanism of TAC-induced pulmonary remodeling and mortality is summarized in Figure 6H. These changes mirror the histological remodeling described in human pulmonary venous hypertension secondary to mitral stenosis and LV failure.^{15–17}

The massive lung fibrosis in this type 2 PH model suggests that an effective treatment of LV end-stage heart failure may require additional efforts to reduce lung fibrosis. In the context of the poor clinical outcome for patients with lung fibrosis, the mission to treat lung fibrosis in type 2 PH model can be very challenging. A team effort from experts in the field of heart failure, PH, and lung fibrosis is likely to be required to achieve optimal treatment of congestive heart

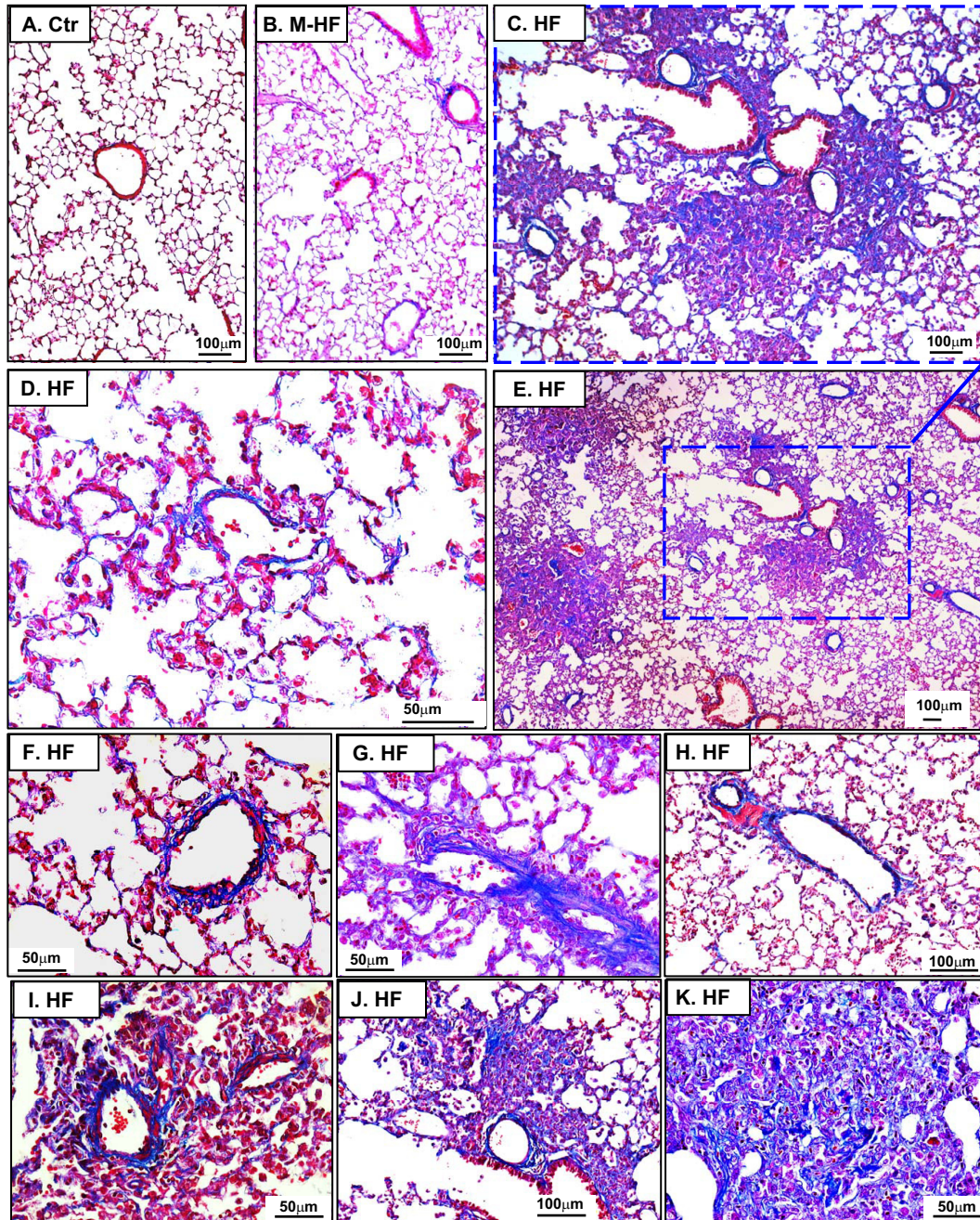


Figure 4. Transverse aortic constriction (TAC)-induced heart failure (HF) causes massive lung fibrosis in mice. Masson Trichrome staining was used to show the relative collagen deposition (the blue staining) in lung tissues from control (A), mild/moderate heart failure (M-HF; B), and HF mice (C through K). B, The general lung structure of M-HF mice is not dramatically changed, but collagen deposition is increased. C through K, Prominent lung vascular or perivascular fibrosis and severe focal fibrosis in collapsed lung tissues in HF mice.

failure. Moreover, the considerable lung fibrosis may be an important mechanism for the poor clinical outcome in patients with end-stage heart failure.

Given the important role for TGF- 1β in lung fibrosis, vascular fibrosis, and fibroblast proliferation, increased lung TGF- 1β mRNA and protein contents in heart failure mice suggest that the TGF- 1β signaling pathway might contribute to the development of lung fibrosis and remodeling in this model. Whether disruption of the TGF- 1β signaling pathway can attenuate the development of lung fibrosis requires further careful investigation.

The pulmonary vascular remodeling, PH, and RV hypertrophy caused by TAC-induced LV failure were greater than that produced by hypoxia (10% oxygen exposure). The increases in lung TGF- 1β , tumor necrosis factor- α , monocyte chemoattractant protein 1, interleukin 1β , toll-like receptor-4, ICAM, and VCAM 1 mRNA or protein content, which have been observed previously in hypoxia-induced PH mice, were also observed in lung tissues from mice with TAC-induced PH. These data indicate that the TAC-induced type 2 PH model shares some characteristics in common with those observed in hypoxia-induced PH in mice. Because ICAM and

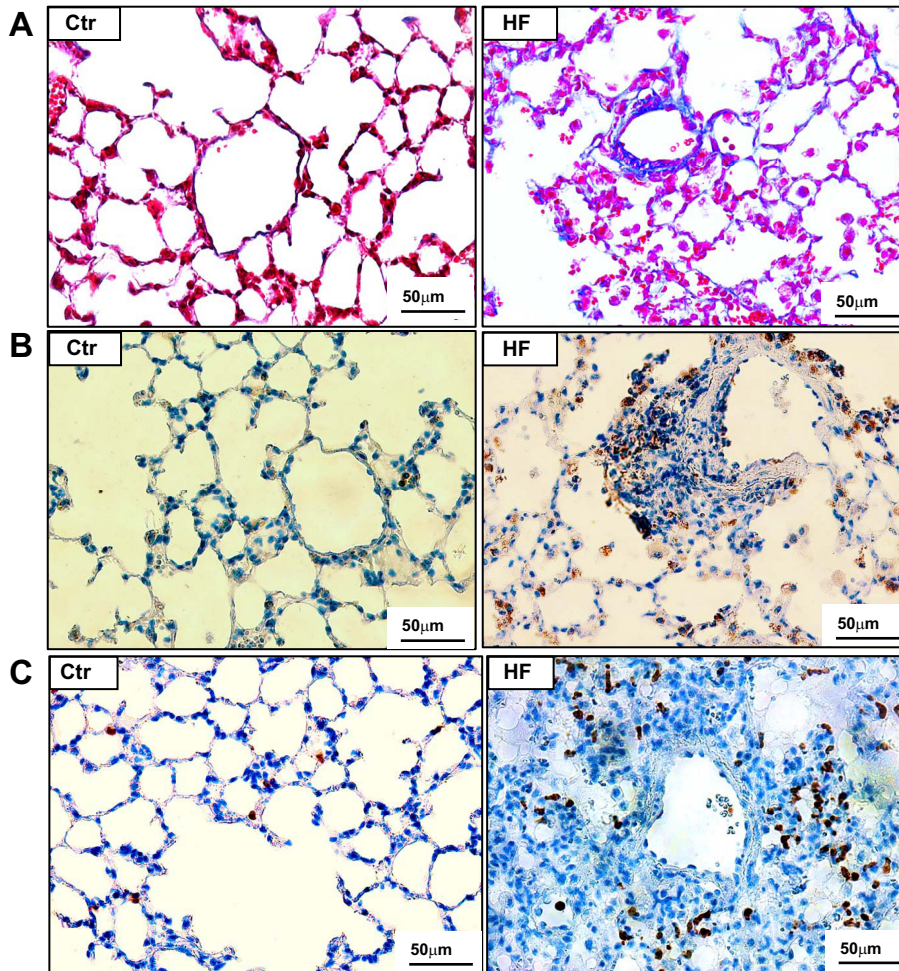


Figure 5. Transverse aortic constriction (TAC)-induced heart failure (HF) causes diffuse lung leukocyte infiltration in mice. **A**, Masson Trichrome staining shows impressive leukocyte infiltration in lung tissues from HF mice compared with controls. **B**, The increased infiltration of macrophages was confirmed by staining with macrophage-specific marker Mac-2, and **(C)** the infiltration of neutrophils was confirmed using an antibody specific for neutrophil clone 7/4.

VCAM facilitate leukocyte-endothelial interaction and leukocyte infiltration, the increased lung ICAM and VCAM proteins in TAC-induced PH mice might be partially responsible for the increased lung leukocyte infiltration. The prominent lung inflammatory response in this type 2 PH model suggests that attenuation of lung inflammation may be a potentially useful approach to treat heart failure and type 2 PH.

There are 2 major limitations for our study. First, although we have not observed any evidence of an increase of lung water content in any of our heart failure mice (mice with either moderate or severe LV dysfunction), it is not clear whether there may have been transient lung edema earlier in the development of the model. Second, the mouse TAC-induced PH model is relatively acute compared with the more chronic course observed in patients with mitral stenosis or LV failure. Therefore, this mouse model may not fully mimic the clinical type 2 PH. Nevertheless, similar histological findings have been described in the clinical situation, suggesting that the TAC-induced PH mouse model is clinically relevant. Moreover, given that thousands of genetically modified mouse strains are currently available and thousands of tissue-specific gene knockout or knock-in mouse strains will be-

come available, the TAC-induced PH mouse model is likely to be a valuable tool to explore molecular mechanisms or novel therapeutic approaches for type 2 PH.

Perspectives

PH secondary to chronic LV failure is classified as type 2 PH. It is predicted that $\leq 60\%$ of patients with severe LV systolic dysfunction and $\leq 70\%$ of patients with LV diastolic dysfunction may develop PH. Understanding the molecular mechanisms for type 2 PH and the development of novel treatments for this condition requires a robust experimental animal model and a good understanding of the nature of the resultant pulmonary remodeling. Here we demonstrate that pressure overload produced by TAC causes a ≤ 5.3 -fold increase in lung wet weight and dry weight, massive pulmonary fibrosis, and type 2 PH in mice. Interestingly, the pressure-overload-induced increase in lung weight was not associated with pulmonary edema but resulted from profound pulmonary remodeling with a dramatic increase in the percentage of fully muscularized lung vessels, marked vascular and lung fibrosis, and leukocyte infiltration. The considerable lung fibrosis, leukocyte infiltration,

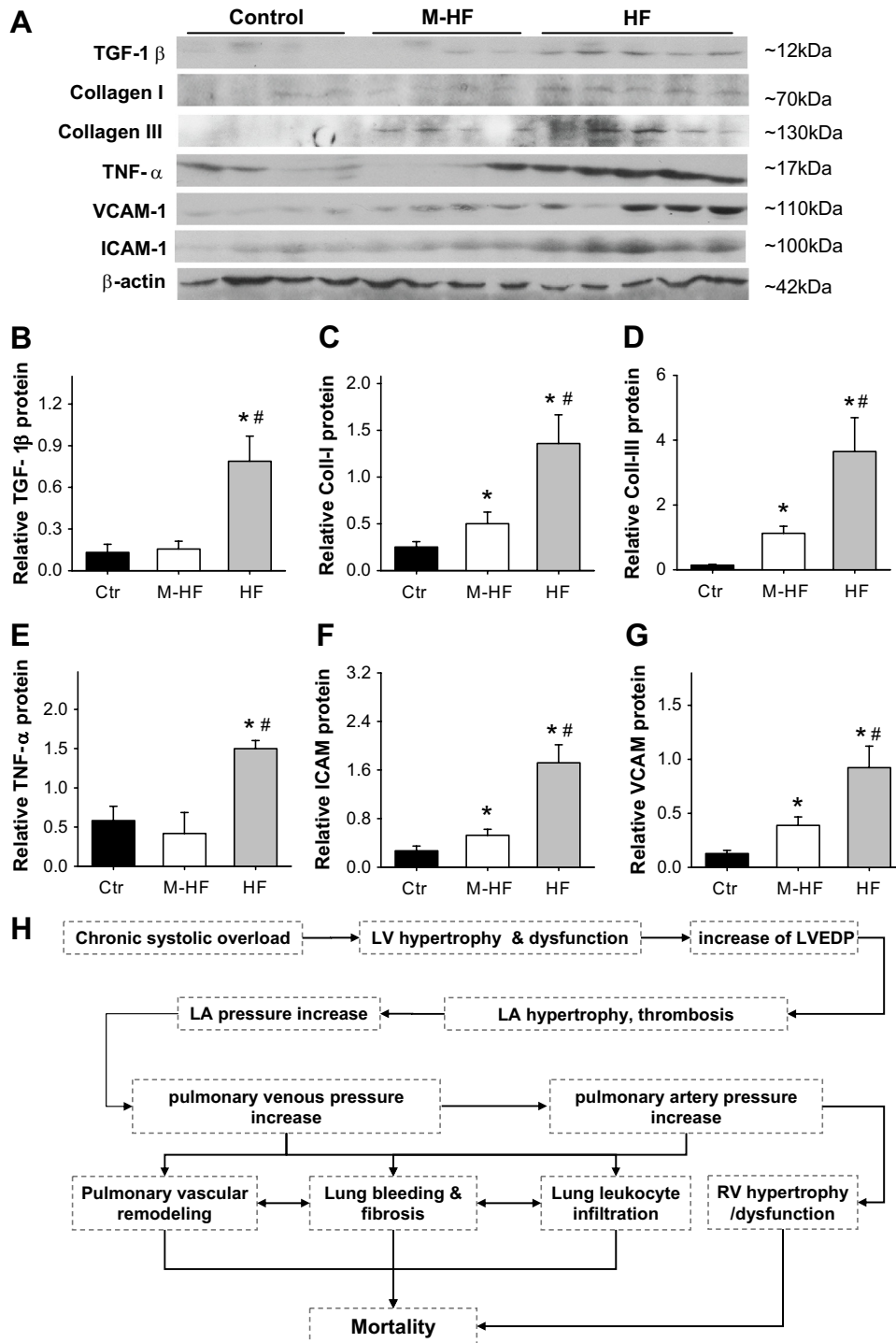


Figure 6. Chronic transverse aortic constriction (TAC) and hypoxia increased expression of genes related to lung fibrosis and inflammation. **A** and **B**, Expression of transforming growth factor (TGF) 1β; **A** and **C**, collagen I; **A** and **D**, collagen III; **A** and **E**, tumor necrosis factor (TNF)-α; and **A**, **F**, and **G**, adhesion molecules intercellular adhesion molecule (ICAM) and vascular cell adhesion molecule (VCAM) in lung tissues from control group, TAC-induced mild/moderate heart failure (M-HF), or heart failure (HF) groups. **H**, The diagram shows the potential mechanism of TAC-induced pulmonary remodeling, pulmonary hypertension, and mortality. **P*<0.05 vs control group; #*P*<0.05 vs corresponding M-HF group.

and PH in mice after pressure overload mimic findings in clinical mitral stenosis and clearly indicate that pulmonary venous hypertension also causes severe lung disease. The massive lung fibrosis may be an important mechanism in the poor clinical outcome in patients with end-stage heart failure. Our findings suggest that the effective treatment of

LV end-stage heart failure may require significant efforts to reduce lung fibrosis and inflammation.

Sources of Funding

This study was supported by US Public Health Service grants R21HL098669, R21HL098719, R21HL102597, RO1HL105406,

1RO1 HL079168, and RO1HL65322 from the National Institutes of Health and Veterans Affairs Research funding.

Disclosures

None.

References

1. Simonneau G, Robbins IM, Beghetti M, Channick RN, Delcroix M, Denton CP, Elliott CG, Gaine SP, Gladwin MT, Jing ZC, Krowka MJ, Langleben D, Nakanishi N, Souza R. Updated clinical classification of pulmonary hypertension. *J Am Coll Cardiol*. 2009;54(1 suppl):S43–S54.
2. Cournaud A, Bloomfield RA, Lauson HD. Double lumen catheter for intravenous and intracardiac blood sampling and pressure recording. *Proc Soc Exp Biol Med*. 1945;60:73–75.
3. Galiè N, Hoeper MM, Humbert M, Torbicki A, Vachiery JL, Barbera JA, Beghetti M, Corris P, Gaine S, Gibbs JS, Gomez-Sanchez MA, Jondeau G, Klepetko W, Opitz C, Peacock A, Rubin L, Zellweger M, Simonneau G. Guidelines for the diagnosis and treatment of pulmonary hypertension. *Eur Respir J*. 2009;34:1219–1263.
4. Hoeper MM, Barberà JA, Channick RN, Hassoun PM, Lang IM, Manes A, Martinez FJ, Naeije R, Olschewski H, Pepke-Zaba J, Redfield MM, Robbins IM, Souza R, Torbicki A, McGoon M. Diagnosis, assessment, and treatment of non-pulmonary arterial hypertension pulmonary hypertension. *J Am Coll Cardiol*. 2009;54(1 suppl):S85–S96.
5. Grigioni F, Potena L, Galiè N, Fallani F, Bigliardi M, Coccolo F, Magnani G, Manes A, Barbieri A, Fucili A, Magelli C, Branzi A. Prognostic implications of serial assessments of pulmonary hypertension in severe chronic heart failure. *J Heart Lung Transplant*. 2006;25:1241–1246.
6. Ghio S, Gavazzi A, Campana C, Inserra C, Klersy C, Sebastiani R, Arbustini E, Recusani F, Tavazzi L. Independent and additive prognostic value of right ventricular systolic function and pulmonary artery pressure in patients with chronic heart failure. *J Am Coll Cardiol*. 2001;37:183–188.
7. Lu Z, Fasset J, Xu X, Hu X, Zhu G, French J, Zhang P, Schnermann J, Bache RJ, Chen Y. Adenosine A3 receptor deficiency exerts unanticipated protective effects on the pressure-overloaded left ventricle. *Circulation*. 2008;118:1713–1721.
8. Lu Z, Xu X, Hu X, Lee S, Traverse JH, Zhu G, Fasset J, Tao Y, Zhang P, dos Remedios C, Pritzker M, Hall JL, Garry DJ, Chen Y. Oxidative stress regulates left ventricular PDE5 expression in the failing heart. *Circulation*. 2010;121:1474–1483.
9. Xu D, Guo H, Xu X, Lu Z, Fasset J, Hu X, Xu Y, Tang Q, Hu D, Somani A, Geurts AM, Ostertag E, Bache RJ, Weir EK, Chen Y. Exacerbated pulmonary arterial hypertension and right ventricular hypertrophy in animals with loss of function of extracellular superoxide dismutase. *Hypertension*. 2011;58:303–309.
10. Lu Z, Xu X, Hu X, Zhu G, Zhang P, van Deel ED, French JP, Fasset JT, Oury TD, Bache RJ, Chen Y. Extracellular superoxide dismutase deficiency exacerbates pressure overload-induced left ventricular hypertrophy and dysfunction. *Hypertension*. 2008;51:19–25.
11. Urboniene D, Haber I, Fang YH, Thenappan T, Archer SL. Validation of high-resolution echocardiography and magnetic resonance imaging versus high-fidelity catheterization in experimental pulmonary hypertension. *Am J Physiol Lung Cell Mol Physiol*. 2010;299:L401–L412.
12. Lu Z, Xu X, Hu X, Fasset J, Zhu G, Tao Y, Li J, Huang Y, Zhang P, Zhao B, Chen Y. PGC-1 α regulates expression of myocardial mitochondrial antioxidants and myocardial oxidative stress after chronic systolic overload. *Antioxid Redox Signal*. 2010;13:1011–1022.
13. Takimoto E, Champion HC, Li M, Belardi D, Ren S, Rodriguez ER, Bedja D, Gabrielson KL, Wang Y, Kass DA. Chronic inhibition of cyclic GMP phosphodiesterase 5A prevents and reverses cardiac hypertrophy. *Nat Med*. 2005;11:214–222.
14. Wang H, Zhang W, Tang R, Hebbel RP, Kowalska MA, Zhang C, Marth JD, Fukuda M, Zhu C, Huo Y. Core2 1–6-N-glucosaminyltransferase-I deficiency protects arteries from neointima formation in ApoE-deficient mice. *Arterioscler Thromb Vasc Biol*. 2009;29:1053–1059.
15. Wagenvoort C, Wagenvoort N. *Pathology of Pulmonary Hypertension. Pulmonary Venous Hypertension*. New York, NY: John Wiley & Sons; 1977:177–216.
16. Wagenvoort CA Lung biopsies and pulmonary vascular disease. In: *Pulmonary Hypertension*. Weir EK, Reeves JT, eds. New York, NY: Futura Publishing Co; 1984.
17. Haworth SG, Hall SM, Panja M. Peripheral pulmonary vascular and airway abnormalities in adolescents with rheumatic mitral stenosis. *Int J Cardiol*. 1988;18:405–416.

ONLINE SUPPLEMENT

Left ventricular failure produces profound lung remodeling and pulmonary hypertension in mice: heart failure causes severe lung disease

Yingjie Chen¹, Haipeng Guo^{1,2}, Dachun Xu^{1,3}, Xin Xu¹, Huan Wang¹, Xinli Hu¹, Zhongbing Lu¹, Dongmin Kwak¹, Yawei Xu³, Roland Gunther⁴, Yuqing Huo¹, E. Kenneth Weir⁵

¹ Lillehei Heart Institute and the Cardiovascular Division, University of Minnesota Medical School, Minneapolis, Minnesota

² Key Laboratory of Cardiovascular Remodeling and Function Research, Qilu Hospital, Shandong University, Shandong, China.

³ Department of Cardiology, Shanghai Tenth People's Hospital, of Tongji University, Shanghai, China

⁴ Research Animal Resources, University of Minnesota Minneapolis, Minnesota

⁵ Department of Medicine, University of Minnesota and Veterans Affairs Medical Center, Minneapolis, Minnesota

Expanded Methods

Induction of PAH with TAC in mice: Male mice at age 10-14 weeks were used for the minimally invasive TAC procedure as we have previously described.^{1,2} Briefly, the mice are anesthetized with a mixture of 80 mg/kg ketamine and 30 mg/kg xylazine (i.p.). The neck and upper ventral chest are shaved, and the mice placed in the supine position. A horizontal incision 5 mm in length is made at the level of the suprasternal notch to allow direct access to the transverse aorta without entering the pleural space. Aortic constriction is performed by ligating the aorta between the right innominate artery and the left carotid artery over a 26-gauge needle using 5.0 silk suture with the aid of a dissecting microscope. The needle is then quickly removed, leaving the constriction in place. The skin is closed using wound clips. Final studies were performed at 8 weeks after TAC.

Induction of PAH with hypoxia in mice: Male C57B6J mice at age 10-14 weeks were exposed to hypobaric hypoxia as previously described.^{3,4} Briefly, the pressure in the chamber was decreased progressively from 0.8 atm (16.9% O₂) on Day 1 to 0.5 atm (10.5% O₂) after Day 7, and was maintained at 10.5% O₂. After exposure to 10.5% O₂ for 2 more weeks, mice were removed from the hypoxia chamber for determination of right ventricular (RV) pressure and hypertrophy. The sham mice were kept in normobaric conditions.

Measurements of aortic pressure, LV and RV hemodynamics: At the end of the study protocol at four weeks, mice were anesthetized with 1.5% isoflurane. They were intubated with a 20-gauge Teflon tube attached to a MiniVent type 845 mouse ventilator (Hugo Sachs Elektronik).¹⁰

A 1.2-F pressure catheter (Scisense Inc. Ontario Canada) was introduced through the right common carotid artery into the ascending aorta for measurement of systolic and diastolic blood pressures, and LV hemodynamics as described previously.^{1,2} For RV hemodynamics, open-chest RV catheterization was performed during anesthesia with 1.5% isoflurane.^{3,5} Data were collected when steady state was reached.

Sample Preparation: After the final hemodynamic assessment, the mice were euthanized by exsanguination, and the heart, lung, and other major organs were harvested. The wet weight of RV and of left ventricle (LV) + septum (S) were weighed and the ratio of RV weight to LV + S was calculated as an index of RV hypertrophy.^{3,6,7} Lung wet weight was determined and the left lung was snap-frozen in liquid nitrogen for biochemical analysis. The airways of the upper right lobe were subsequently perfused and fixed in 10% buffered formalin for histological analysis. Visual comparable inflation of the lung lobes were observed in all tissues.

Histological staining: The relative pulmonary vascular muscularization was determined under H&E staining. Briefly, in each mouse, 60 intra-acinar arteries were examined and categorized as nonmuscular (NM), partially muscular (PM) or fully muscular (FM). The relative percentage of NM, PM and FM arteries was calculated. Lung fibrosis was stained using Masson's Trichrome Stain Kit from Sigma-Aldrich. Heart sections were stained with Sirius Red (Sigma) for fibrosis, and FITC conjugated wheat germ agglutinin (AF488, Invitrogen, Carlsbad, CA) to evaluate myocyte size using methods as previously described.^{1,2,3,8}

In addition, lung sections were stained with monoclonal antibodies to identify smooth muscle cells or myofibroblasts (using an antibody anti-mouse smooth muscle α -actin, Sigma-Aldrich),² macrophages (using an antibody against Mac-2, clone M3/38; Accurate Chemical, Westbury),⁹ and neutrophils (using anti-mouse neutrophil antibody clone 7/4; Accurate Chemical).⁹ Briefly, tissue sections (5 μ m) were deparaffinized, rehydrated and antigen recovered in Tris-EDTA buffer (pH=9.0) for 30 minutes at 95-100°C before being washed in PBS. The sections were incubated with 3% H₂O₂ in PBS for 20 minutes, followed by 3% BSA solution for 1 hour. Sections were then incubated with corresponding monoclonal primary antibodies (1:400) overnight at 4°C, and followed with avidin/biotin peroxidase-linked secondary antibody (1:1000) (Invitrogen).⁹ Staining was visualized by using an avidin/biotin peroxidase-linked detection system (Vector Laboratories, Burlingame, CA).

Measure lung water content: Lung (lower right lobe) wet weight was first determined. The lung tissue was then dried at 58°C to a constant weight. The dry weight of lung tissue was then determined. The relative water content of lung tissue was calculated using the following equation: Lung water content = (lung wet weight – lung dry weight)/lung wet weight X 100%.

Quantitative RT-PCR: Isolation of total RNA from lung and determination of cDNA synthesis by reverse transcription and quantitative real-time PCR were performed as described previously.³ Briefly, total RNA was isolated from lung tissue and reverse-transcribed using the High-Capacity cDNA Reverse Transcription Kit (Applied Biosystems). Quantitative real-time PCR reaction was performed using the Fast SYBR® Green Master Mix (Applied Biosystems). Results were normalized to 18S rRNA levels. The sequences of the primers are provided in **Table S1**.

Statistical Analysis: Values of each group are expressed as mean \pm standard error. Data of two groups was compared with unpaired t-test. One-way ANOVA was used to test for differences among groups. If analysis of variance demonstrated a significant effect, *post hoc* pair-wise comparisons were made using the Fisher least significant difference test. Statistical significance was defined as $p < 0.05$.

References

1. Lu Z, Fassett J, Xu X, Hu X, Zhu G, French J, Zhang P, Schnermann J, Bache RJ, Chen Y. Adenosine A3 receptor deficiency exerts unanticipated protective effects on the pressure-overloaded left ventricle. *Circulation*. 2008;118:1713-1721.
2. Lu Z, Xu X, Hu X, Lee S, Traverse JH, Zhu G, Fassett J, Tao Y, Zhang P, dos Remedios C, Pritzker M, Hall JL, Garry DJ, Chen Y. Oxidative stress regulates left ventricular PDE5 expression in the failing heart. *Circulation*. 2010;121:1474-1483.
3. Xu D, Guo H, Xu X, Lu Z, Fassett J, Hu X, Xu Y, Tang Q, Hu D, Somani A, Geurts AM, Ostertag E, Bache RJ, Weir EK, Chen Y. Exacerbated pulmonary arterial hypertension and right ventricular hypertrophy in animals with loss of function of extracellular superoxide dismutase. *Hypertension*. 2011;58:303-309.
4. Hampl V, Tristani-Firouzi M, Nelson DP, Archer SL. Chronic infusion of nitric oxide in experimental pulmonary hypertension: pulmonary pressure-flow analysis. *Eur Respir J*. 1996;9:1475-1481.
5. Lu Z, Xu X, Hu X, Zhu G, Zhang P, van Deel ED, French JP, Fassett JT, Oury TD, Bache RJ, Chen Y. Extracellular superoxide dismutase deficiency exacerbates pressure overload-induced left ventricular hypertrophy and dysfunction. *Hypertension*. 2008;51:19-25.
6. Handoko ML, de Man FS, Happé CM, Schaliij I, Musters RJ, Westerhof N, Postmus PE, Paulus WJ, van der Laarse WJ, Vonk-Noordegraaf A. Opposite effects of training in rats with stable and progressive pulmonary hypertension. *Circulation*. 2009;120:42-49.
7. Urboniene D, Haber I, Fang YH, Thenappan T, Archer SL. Validation of high-resolution echocardiography and magnetic resonance imaging versus high-fidelity catheterization in experimental pulmonary hypertension. *Am J Physiol Lung Cell Mol Physiol*. 2010;299:L401-L412.
8. Lu Z, Xu X, Hu X, Fassett J, Zhu G, Tao Y, Li J, Huang Y, Zhang P, Zhao B, Chen Y. PGC-1 α regulates expression of myocardial mitochondrial antioxidants and myocardial oxidative stress after chronic systolic overload. *Antioxid Redox Signal*. 2010;13:1011-1022.
9. Wang H, Zhang W, Tang R, Hebbel RP, Kowalska MA, Zhang C, Marth JD, Fukuda M, Zhu C, Huo Y. Core2 1-6-N-glucosaminyltransferase-I deficiency protects injured arteries from neointima formation in ApoE-deficient mice. *Arterioscler Thromb Vasc Biol*. 2009;29:1053-1059.

Table S1. Primers for real-time RT-PCR products.

Genes	Sense	Antisense
TGF- β	5'-CTGATACGCCTGAGTGGCTGTC-3'	5'-AGCGAAAGCCCTGTATTCCG-3'
Collagen I	5'-CATAAAGGGTCATCGTGGCT-3'	5'-TTGAGTCCGTCTTTGCCAG-3'
Collagen III	5'-GAAGTCTCTGAAGCTGATGGG-3'	5'-TTGCCTTGCGTGTTTGATATTC-3'
TNF- α	5'-TGGGCTCCCTCTCATCAGTTC-3'	5'-GGCTACGGGCTTGCTCACTCG-3'
MCP-1	5'-CAAGATGATCCCAATGAGTCG-3'	5'-CTTCTTTGGGACACCTGCTGCT-3'
TLR4	5'-TTCAGAACTTCAGTGGCTGG-3'	5'-TGTTAGTCCAGAGAACTTCCTG-3'
IL-1 β	5'-CCTCTCAAGCAGAGCACAGACC-3'	5'-TGGTGAAGTCAACTATGTCCCG-3'
VCAM	5'-ACAAAGGCAGAGTACACAGAC-3'	5'-CACAGGATTTTGGGAGTTGG-3'
ICAM	5'-GAGAAGTTGGACAGAACCCTG-3'	5'-GTTACTTGGTCCCCTTCTGAG-3'
18S	5'-AGTCCCTGCCCTTTGTACACA-3'	5'-CGATCCGAGGGCCTCACTA-3'
GAPDH	5'-TCCTGCACCACCAACTGCTTAG-3'	5'-GATGACCTTGCCCACAGCCTTG-3'

Table S2. Anatomic data of control, M-HF, HF and hypoxia groups.

Parameters	Control	M-HF	HF	Hypoxia
Number of mice	10	11	10	11
Bodyweight (g)	28.0±0.88	29.3±0.67	27.1± 0.69	28.0 ±0.48
Tibia length (mm)	17.9±0.10	18.1±0.08	18.1±0.10	17.9±0.05
Left ventricular + septum weight (mg)	97.3±2.36	162±8.93*	187±4.87*†	99.6±4.01
Left atria weight (mg)	3.17±0.17	9.54±1.12*	16.3±2.53*†	3.21±0.13
Lung mass (mg)	139±2.88	185±16.1*	395±23.4*†	187±3.00*
Right ventricular weight (mg)	21.9±0.79	26.9±1.96	38.8±1.1.93*†	34.6±2.04*
Right atria weight (mg)	3.61±0.18	4.61±0.47	6.01±0.57*†	3.55±0.15
Ratio of RV weight to LV weight	0.23±0.01	0.165±0.01*	0.21±0.01†	0.35±0.01*
Ratio of RA weight to LA weight	1.19±0.01	0.52±0.05*	0.49±0.07*	1.13±0.07
Ratio of left ventricular weight to body weight (mg/g)	3.48±0.06	5.50±0.21*	6.87±0.13*†	3.55±0.10
Ratio of LA weight to body weight (mg/g)	0.11±0.01	0.32±0.03*	0.59±0.09*†	0.12±0.01
Ratio of lung weight to body weight (mg/g)	4.99±0.12	6.33±0.18*	14.7±0.89*†	6.68±0.09*
Ratio of right ventricular weight to body weight (mg/g)	0.79±0.04	0.91±0.06	1.43±0.08*†	1.23±0.06*
Ratio of RA weight to body weight (mg/g)	0.13±0.01	0.15±0.02	0.22±0.02*†	0.13±0.01
Ratio of left ventricular weight to tibia length (mg/mm)	5.44±0.11	8.96±0.48*	10.4±0.28*†	5.56±0.23
Ratio of LA weight to tibia length (mg/mm)	0.18±0.01	0.53±0.06*	0.90±0.14*†	0.18±0.01
Ratio of lung weight to tibia length (mg/mm)	7.78±0.14	10.2±0.87*	21.9±1.32*†	10.4±0.18*
Ratio of right ventricular weight to tibia length (mg/mm)	1.22±0.04	1.49±0.11	2.16±0.11*†	1.94±0.12*

*p<0.05 as compared with corresponding control conditions; † p<0.05 as compared with LVH.

Table S3. Hemodynamic of mice in control group, mild heart failure group (M-HF), severe heart failure group (HF), or hypoxia group.

parameters	Control	M-HF	HF	Hypoxia
Number of mice	6	10--12	5--8	7-10
Heart rate (beats per minute)	518±11.2	553±10.1	562±10.5	553±10.1
RV systolic pressure (mmHg)	21.3±1.02	38.7±3.54*	55.1±8.46*†	43.0±1.52*
RV end diastolic pressure (mmHg)	1.25±0.11	3.15±1.06	8.37±5.01*†	2.63±0.18*
LV systolic pressure (mmHg)	117±1.36	171±4.52*	149±9.75*†	117±5.3
LV end diastolic pressure (mmHg)	6.12±0.90	11.7±2.12*	24.5±1.59*†	8.17±4.0

*p<0.05 as compared with corresponding control conditions; † p<0.05 as compared with M-HF.

Expanded Results

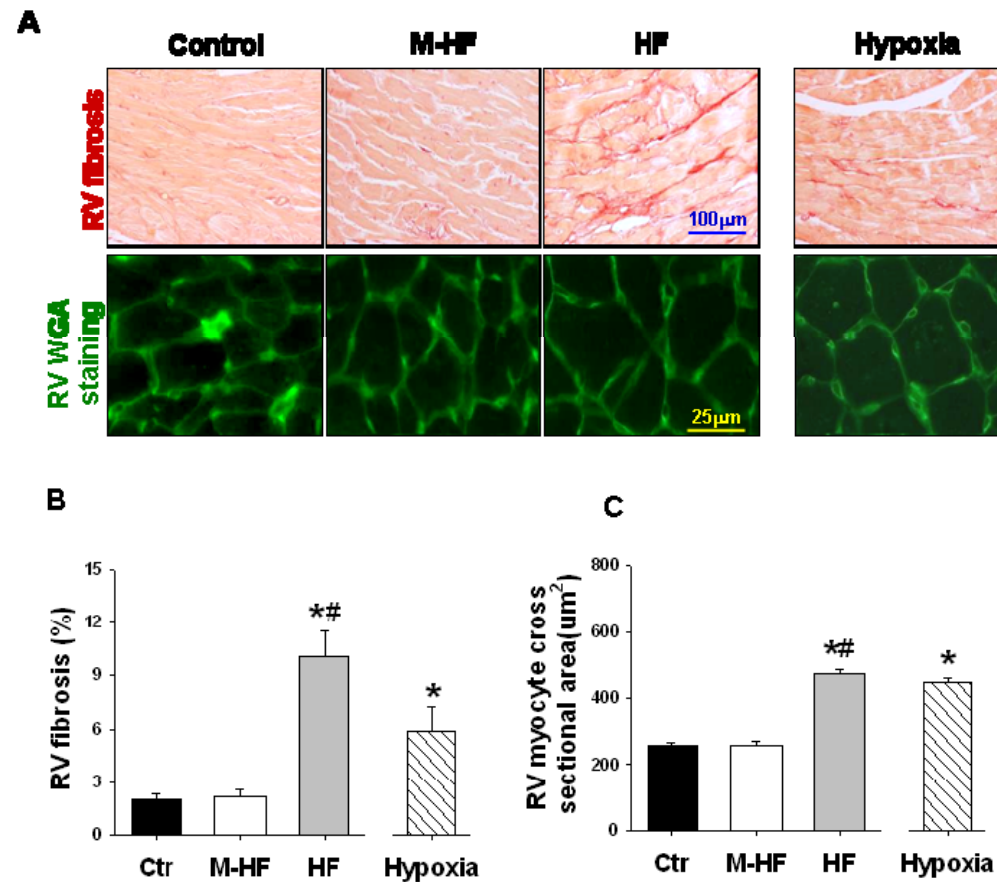


Figure S1. Relative RV fibrosis and RV cardiac myocyte hypertrophy in 4 experimental groups. Increased RV fibrosis is observed in hypoxia group and HF group (A,B). Increased RV cardiac myocyte size in hypoxia group and HF group (A, C). * $p < 0.05$ vs control group; # $p < 0.05$ vs. corresponding M-HF group.

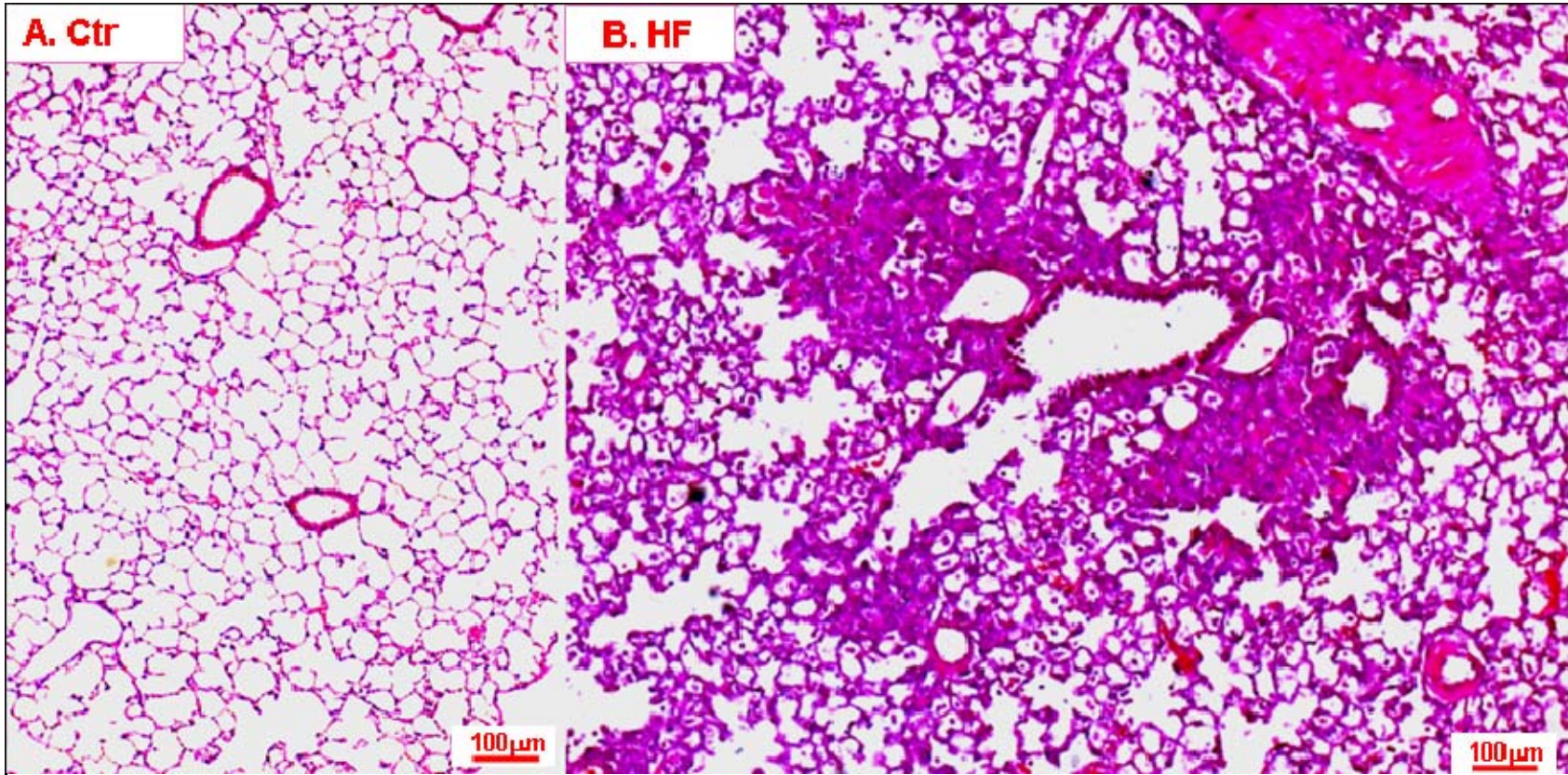


Figure S2. Representative H&E stained lung section shows increased pulmonary vascular wall thickness, and focal collapsed lung tissue in a HF mouse relative to control.

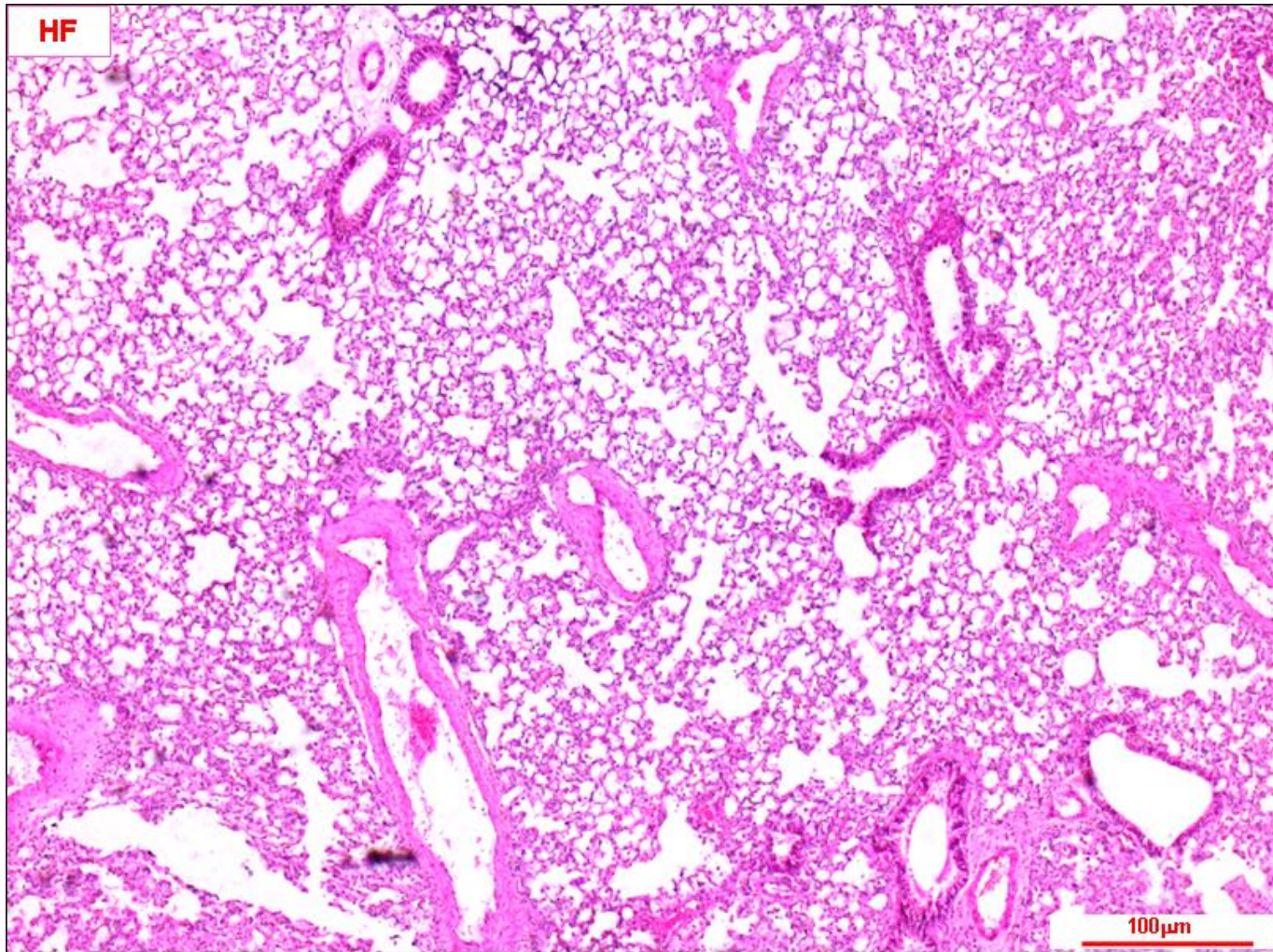


Figure S3. Representative H&E stained lung section shows marked pulmonary vascular remodeling in a HF mouse.

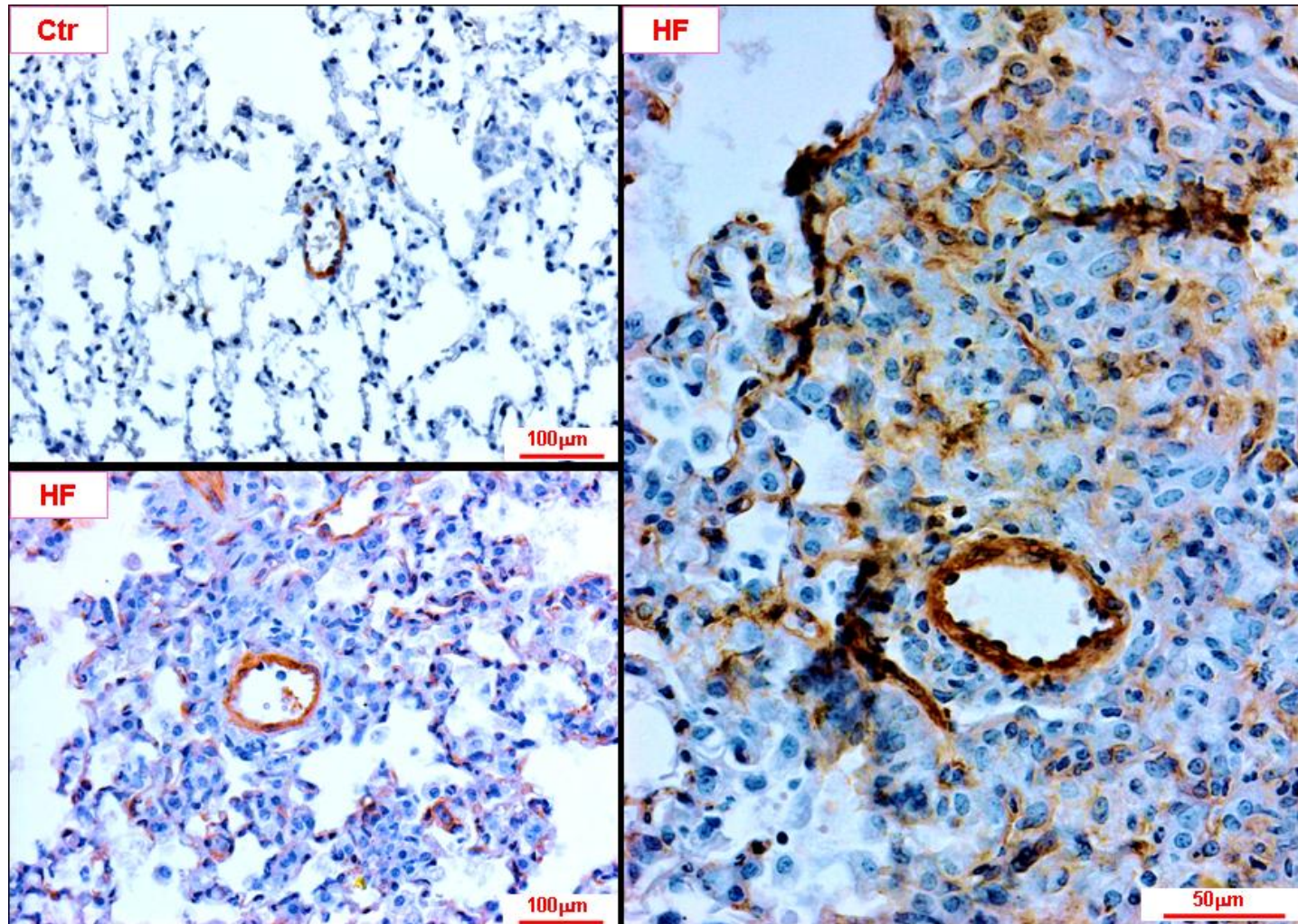


Figure S4. Representative lung sections show increased staining for smooth muscle α -actin in pulmonary vessels and collapsed lung tissue in HF mice, indicating proliferation of smooth muscle cells and myofibroblasts in lung tissues.

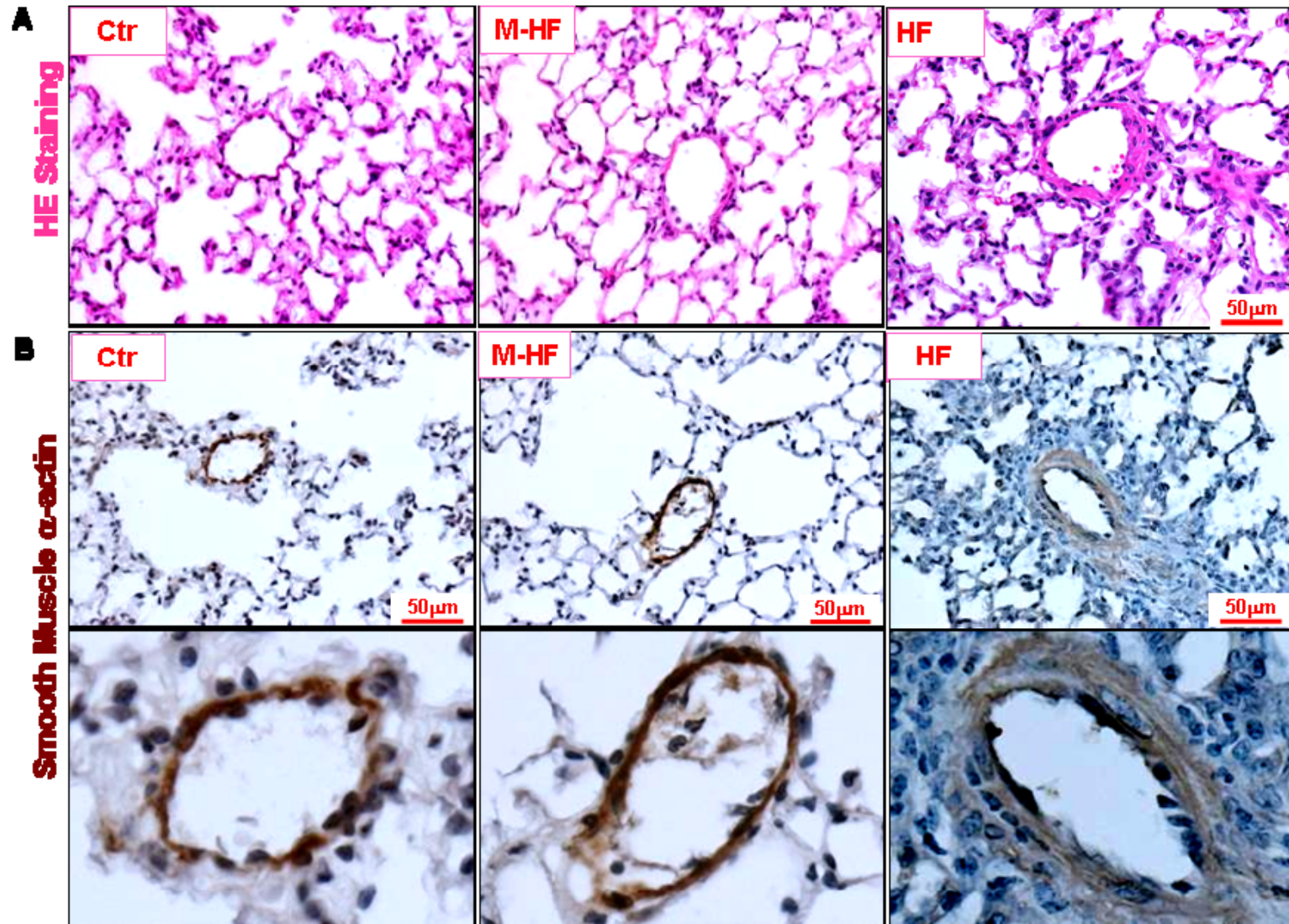


Figure S5. (A) Representative H&E stained sections show small arteries in control, M-HF and HF mice. (B) Representative staining of smooth α -actin shows increased proliferation of smooth muscle cells and/or myofibroblast in HF mice.

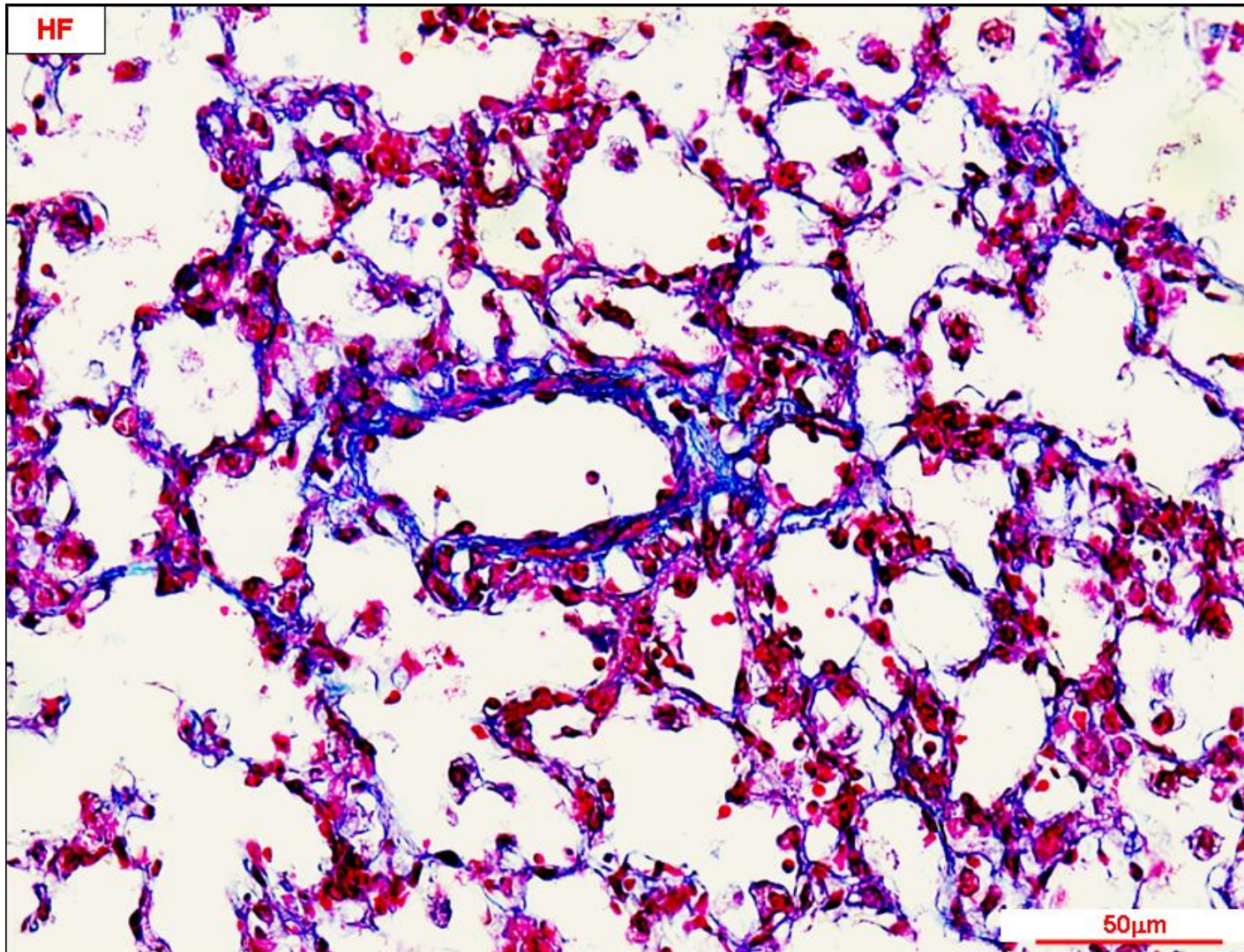


Figure S6. Representative Masson's Trichrome stained lung section shows widespread collagen deposition (blue staining) in the lung interstitial space and vessels in a HF mouse.

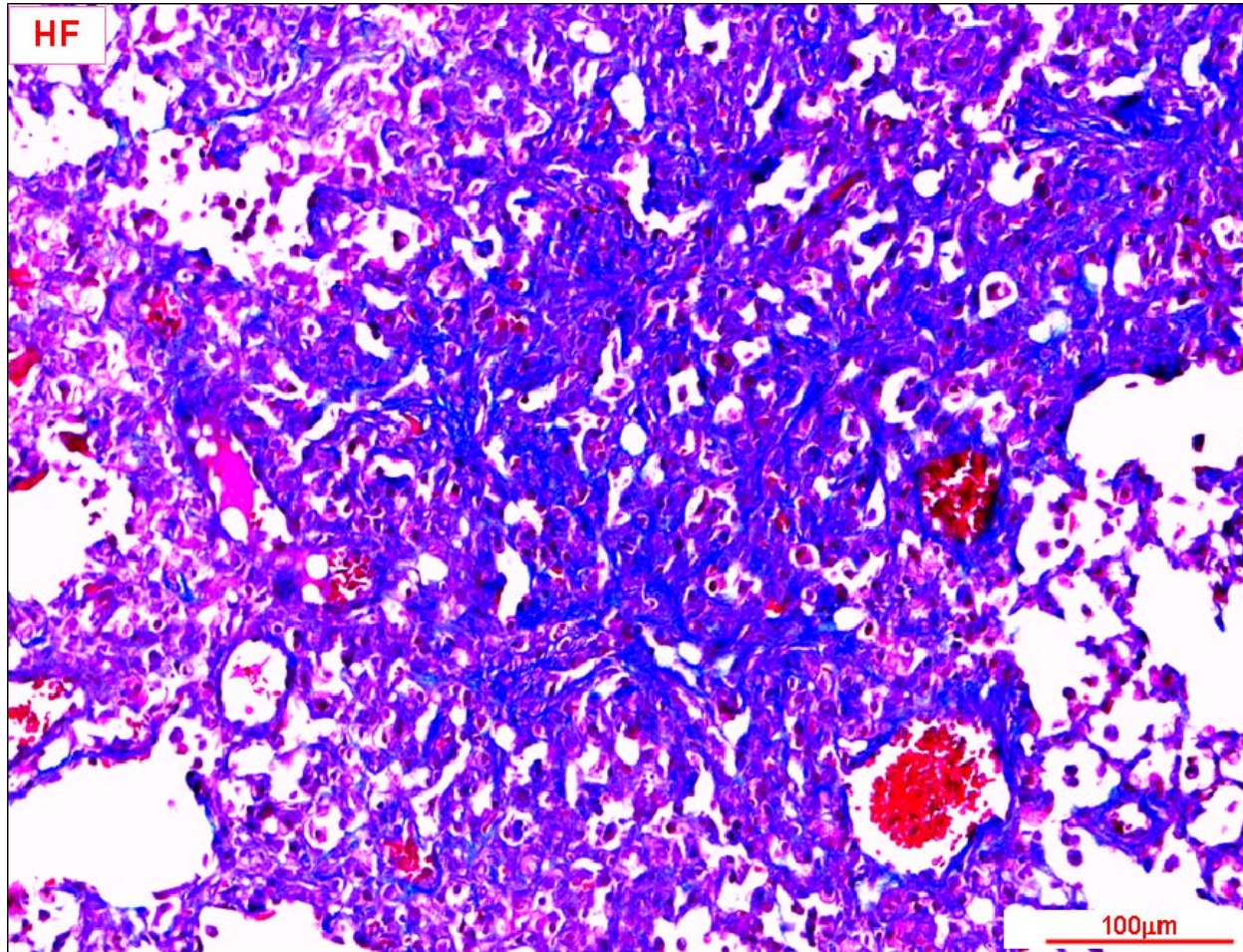
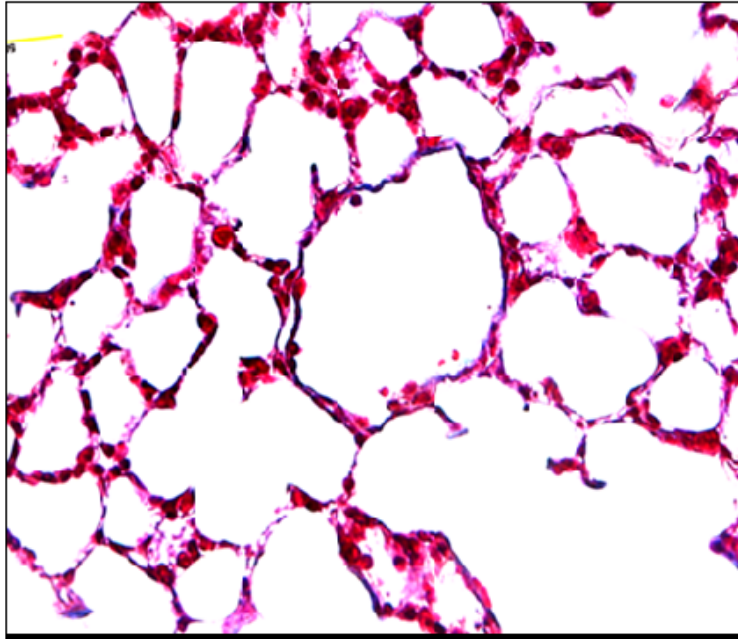


Figure S7. Masson's Trichrome stained lung section shows dense focal collagen deposition (blue staining) in the lung interstitial space and vessels in a HF mouse.

Normal Lung



Heart Failure Lung

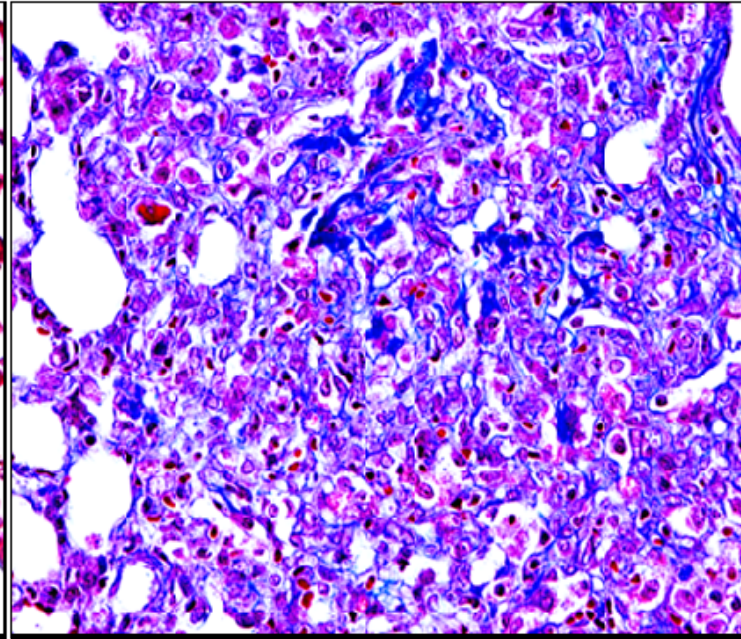


Figure S8. Masson's Trichrome stained lung sections show the destruction of normal lung structure and the dramatic focal collagen deposition (blue staining) in a mouse with severe heart failure.

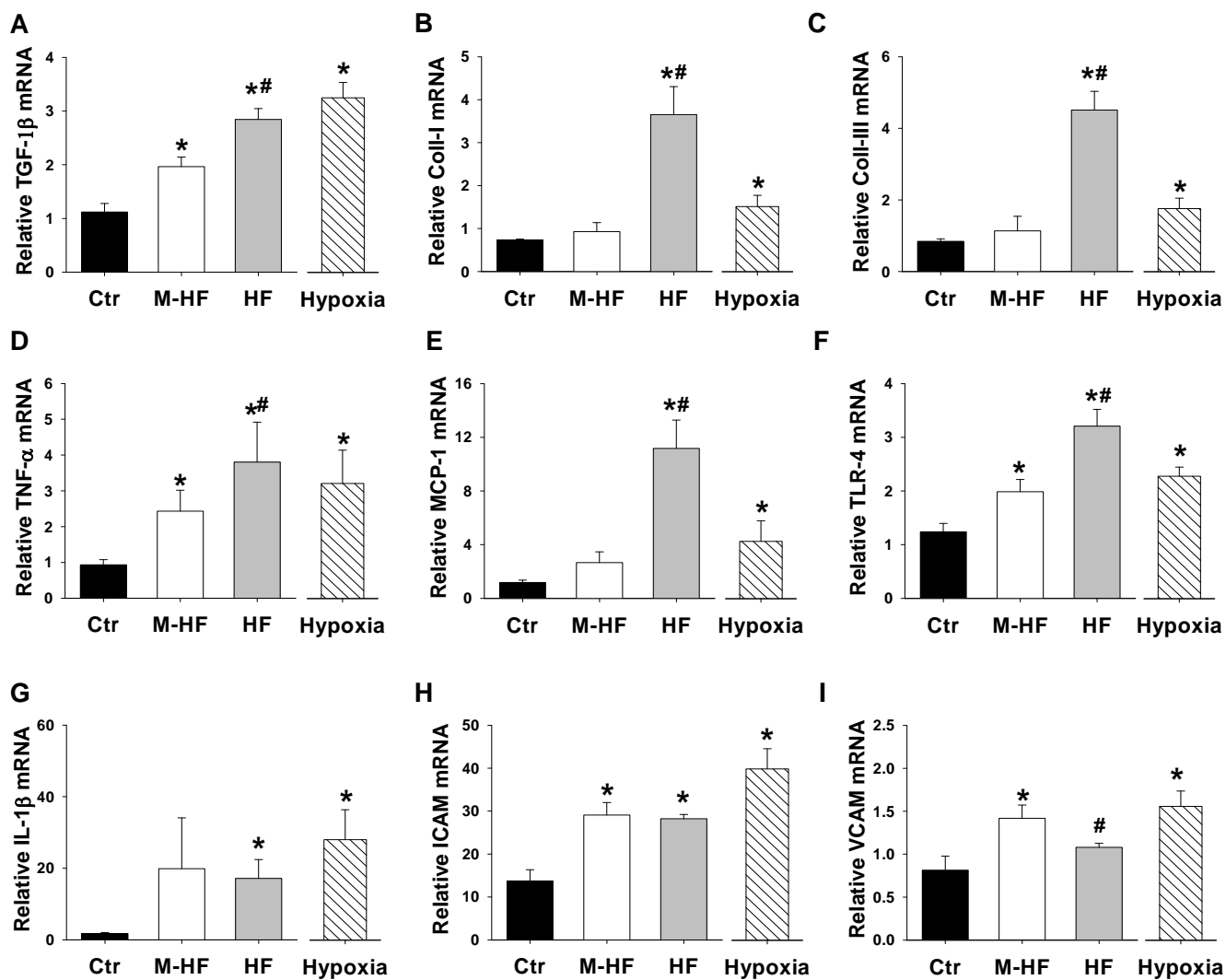


Figure S9. Chronic TAC and hypoxia increased expression of genes related to lung fibrosis and inflammation. (A) Expression of TGF-1 β ; (B) Collagen-I; (C) collagen-III; (D-F) pro-inflammatory cytokines; and (G-I) adhesion molecules ICAM and VECAM in lung tissues from control group, TAC-induced LVH or CHF groups, and hypoxia group. * $p < 0.05$ vs control group; # $p < 0.05$ vs. corresponding LVH group